Nuclear Science and Techniques (2025) 36:108
https://doi.org/10.1007/s41365-025-01738-9

Laser-driven micro-pinch: a pathway to ultra-intense neutrons

Pu-Tong Wang[1] · Xue-Song Geng[2] · Guo-Qiang Zhang[3] · Liang-Liang Ji[4] · Yu-Gang Ma[5]

Received: 12 February 2025 / Revised: 14 March 2025 / Accepted: 18 March 2025 / Published online: 2 May 2025

Abstract
Utilizing the laser-driven Z-pinch effect, we propose an approach for generating an ultrashort, intense MeV neutron source with femtosecond pulse duration. The self-generated magnetic field driven by a petawatt-class laser pulse compressed the deuterium in a single nanowire to more than 120 times its initial density, achieving an unprecedented particle number density of 10^{25} cm^{-3}. Through full-dimensional kinetic simulations, including nuclear reactions, we found that these Z-pinches can generate high-intensity and short-duration neutron pulses, with the peak flux reaching 10^{27} cm^{-2}s^{-1}. Such laser-driven neutron sources are beyond the capabilities of existing approaches and pave the way for groundbreaking applications in r-process nucleosynthesis studies and high-precision time-of-flight neutron data measurements.

Keywords Nanowire target · Z-pinch · D–D fusion reaction · Laser plasma · Neutron source

1 Introduction

Conventional neutron sources, which include the isotope, accelerator, and reactor types, have played pivotal roles in advancing diverse scientific and technological domains such as materials science and nuclear physics [1]. Spallation neutron sources, which represent the forefront of this evolution, constitute a novel generation of high-intensity pulsed neutron sources. They have achieved neutron flux levels of approximately 10^{17} cm^{-2}s^{-1} with short pulse widths. These attributes significantly enhance the precision of time-of-flight (TOF) measurements, which are a cornerstone of nuclear reactor design and nuclear astrophysics [2–5].

Despite these advancements, replicating high-neutron-flux conditions, which are crucial for understanding r-process nucleosynthesis [6], remains a formidable challenge. In the cosmic formation of heavy elements, neutron star mergers are the primary site of this process [7], whereas the contribution from supernovae explosions is still under debate [8]. These astrophysical events require specific conditions, including an intensive neutron flux ranging from 10^{22} to 10^{28} cm^{-2}s^{-1}, a range that remains elusive in laboratory settings. This gap not only hinders our comprehensive understanding of these astrophysical phenomena but also limits advancements in related fields, such as nuclear physics and astrophysics. Therefore, the development of new

Pu-Tong Wang and Xue-Song Geng contributed equally to this work.

This work was supported by the National Key R&D Program of China (Nos. 2022YFA1602402, 2022YFA1602404) and the National Natural Science Foundation of China (Nos. 12235003,12388102).

✉ Guo-Qiang Zhang
zhangguoqiang@sari.ac.cn

Liang-Liang Ji
jill@siom.ac.cn

Yu-Gang Ma
mayugang@fudan.edu.cn

[1] Shanghai Institute of Applied Physics, Chinese Academy of Sciences, Shanghai 201800, China

[2] University of Chinese Academy of Sciences, Beijing 100049, China

[3] State Key Laboratory of High Field Laser Physics and CAS Center for Excellence in Ultra-intense Laser Science, Shanghai Institute of Optics and Fine Mechanics, Chinese Academy of Sciences, Shanghai 201800, China

[4] Shanghai Advanced Research Institute, Chinese Academy of Sciences, Shanghai 201210, China

[5] Key Laboratory of Nuclear Physics and Ion-Beam Application (MOE), Institute of Modern Physics, Fudan University, Shanghai 200433, China

methodologies capable of achieving these extreme conditions in a controlled environment is crucial.

The recent development of laser-driven high-intensity neutron sources has shown the potential to fill this gap owing to their exceptional temporal resolution and ability to achieve highly localized neutron beams (spatial resolution) [9, 10]. These sources employ various methodologies, including photoneutron production [11, 12] (10^{21} $cm^{-2}s^{-1}$), target normal sheath acceleration (TNSA) [13, 14] (10^{24} $cm^{-2}s^{-1}$), and target compression via spherical shells (NIF) [15] (10^{30} $cm^{-2}s^{-1}$). Although these methods offer advancements, the neutron flux from the laser-driven Z-pinch has the potential to surpass the current capabilities.

Z-pinch is a phenomenon in which an axial current flowing through a plasma generates a magnetic field. The interaction between this magnetic field and the current creates a radial Lorentz force, which radially compresses the plasma to a small volume [16]. Fusion and X-ray studies have also explored the potential of Z-pinch devices [17–20]. Recent studies have focused on augmenting laser-driven Z-pinch mechanics using nanowire arrays [21–23], which present notable intrigues. Nanowire arrays efficiently absorb the energy from a femtosecond petawatt laser, resulting in a high degree of ionization and intense X-ray generation [24, 25]. In addition, ions in the array are accelerated, triggering microscale fusion reactions [26].

Therefore, we performed a particle-in-cell (PIC) simulation and found that a femtosecond petawatt laser can pinch a single nanowire to more than 120 times its original density. It is referred to as a micro-pinch, owing to its small spatial scale and short duration. Simulations suggest that these micro-pinches can facilitate nuclear fusion reactions, leading to an intense, short-lived neutron pulse with an unprecedented flux of 10^{27} $cm^{-2}s^{-1}$.

2 Simulation setting

To investigate the neutron generation process in a Z-pinch setup, we employed full-dimensional kinetic simulations to reveal the ultrashort pinch process and the generation of neutrons using the PIC code Smilei [27]. The original nuclear reaction scheme [28, 29] was introduced in Smilei. Specifically, the cross section for the reaction D + D→ n + ^{3}He was integrated into the debugging version of Smilei. We improved the debugging version and corrected and checked the nuclear reaction cross sections using a period boundary condition in a box [30]. In addition, we added the nuclear reaction D + T → n + ^{4}He (data from [31]) to determine the potential for a higher-intensity neutron source.

In our simulation, the nanowire where Z-pinch was triggered was composed of deuterated polyethylene (CD_2). The particle number density of deuterium was set as $\rho = 7.8 \times 10^{22}$ cm^{-3}. Diameters of 300 and 500 nm were considered for varying wire lengths. The initial temperature of the particles was 300 Kelvin. The nanowire target was irradiated by 400 nm wavelength circularly polarized (CP) laser pulses of 30 or 60 fs full width at half maximum (FWHM) duration. The dimensionless amplitude of the laser field was $a_0 = 10 - 40$ ($a_0 = eE/m_e c\omega$), where e and m_e are the electron charge and mass, E is the laser electric field, ω is the laser frequency, and c is the speed of light in vacuum. The focal spot size of the laser should be sufficiently large to cover an entire single nanowire. The typical focal spot size was approximately 5 µm, reaching a peak intensity of $\sim 5 \times 10^{21}$ W/cm^2 ($a_0 = 17$). To avoid numerical heating, the size and number of cells were dynamically adjusted according to the volume of the nanowires. A typical cell size was set to 7.5 nm × 5 nm × 5 nm, with 27 macroparticles per cell. A small nanowire had 640 × 192 × 192 cells, corresponding to a cube of 4.8 µm × 0.96 µm × 0.96 µm, which was sufficiently large to hold the entire nanowire. The simulation boundaries were set to open conditions for both the fields and particles. Because field ionization is the dominant ionization process compared with that from Coulomb collisions between particles, collisional ionization was switched off to save simulation time. The binary collision between deuterium (tritium) was set, as nuclear reactions might occur.

3 Simulation result

When irradiated with ultrashort high-intensity laser pulses, the atoms inside the wire undergo field ionization. The ionization process leads to a considerable potential difference on the surface of the nanowire. This potential disparity is balanced by the significant return current flowing across the nanowire's surface, maintaining quasi-neutrality. For an approximate estimation, we assumed that the electrons ionized from atoms within the nanowire were mostly distracted by the laser, corresponding to a total charge of $Q = 1.3 \times 10^{-8}$ C. The current can be calculated as $I = Q/t$, where t represents the FWHM duration of the laser, which is set to 60 fs. This estimated current of 2.2×10^5 A provides a starting point for further analysis of the Z-pinch dynamics.

We performed three-dimensional (3D) simulations to illustrate the laser-induced Z-pinch process. Figure 1 shows that the electrons are pulled out by the CP laser in the void (negative current represented in blue), whereas the positive current density is the return current of the electrons flowing in the opposite direction (positive current represented in red). The return current density reached $J = 10^{15}$ A/cm^2 – 10^{16} A/cm^2 (a cross section of 30 nm × 30 nm, $I_{max} \sim 1.4 \times 10^5$ A), which is consistent

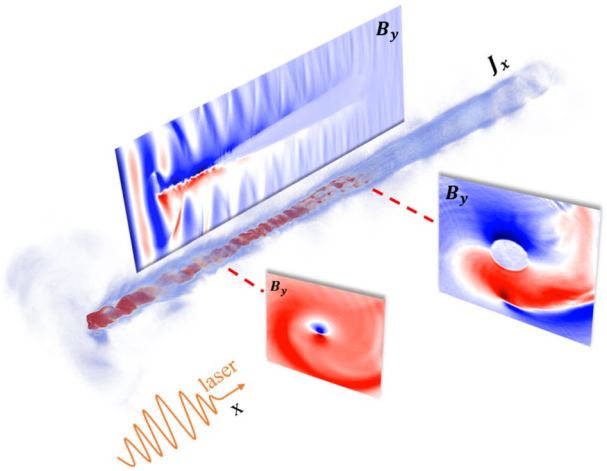

Fig. 1 (Color online) 3D current density and 2D magnetic fields during the pinch simulation. In the 3D image, the red color represents positive current (max $J_x = 1.4 \times 10^{16}$ A/cm^2), whereas the blue color represents negative current. The 2D image illustrates the magnetic field (max $B_y = 1.0 \times 10^6$ T). The x-positive direction aligns with the laser propagation and the axial direction of the nanowire, whereas the y and z directions correspond to the radial directions of the nanowire

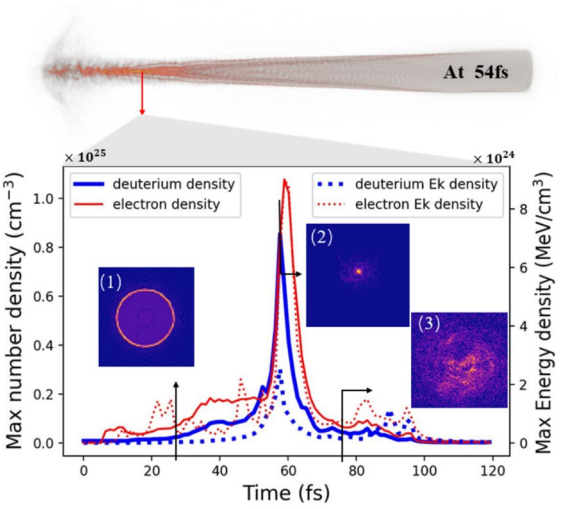

Fig. 2 (Color online) Spatial and temporal profile of plasma density and energy density. The profile at 1.2 μm is shown from the top of the nanowire. The time-dependent variation of deuterium is depicted along the curve graph, specifically at the section indicated in blue, and red denotes electrons. The dotted lines denote the time-dependent variation of energy density. Sub-fig(2) demonstrates the deuterium number density after compression, which reaches a value of approximately 8×10^{24} cm^{-3}

with the estimation. Because of the extremely high current density, the induced magnetic field around the nanowire was also significant. The 2D image in Fig. 1 illustrates the transverse magnetic field distribution in the simulation. The maximum field reached $B_y = 1.0 \times 10^6$ T, which exceeded the incident laser field ($a_0 = 17$, $B_y = 4.6 \times 10^5$ T). This quasi-static magnetic field exerted a $J \times B$ force on both the inner and outer currents (electrons) of the nanowire. The current on the inner surface of the nanowire was subjected to a force radially inward owing to the generated magnetic field, whereas the forces on the outer electrons of the nanowire were in opposite directions. Hence, the nanowire was compressed inward, whereas the electrons extracted from the nanowire were pushed outward.

When the return electrons are pinched radially inward by the Lorentz force, they induce an electric field owing to charge separation. Deuterium ions are then drawn and pinched symmetrically inward from the surface by this electric field, resulting in a strong radial symmetry for the kinetic energy distribution of deuterium particles within the nanowire. In the following discussion, we estimated that the temperature of deuterium in the Z-pinch was 190 keV by comparing the ratios of the nuclear reaction rates. The electrons extracted from the nanowire (which were being pushed outward) also induced an electric field, drawing the surface deuterium outward and accelerating them. If the target is an array, the collisions between them are also significant for nuclear reactions because of their higher energies. Eventually, the pinched-inward ions are compressed near the center, creating a high-density zone (Fig. 2). The corresponding maximum energy density can reach an order of 1×10^{24} MeV/cm^3 (1×10^{12} J/cm^3) at approximately 54 fs, which is two orders of magnitude higher than that reported in our previous work [32].

As shown in Fig. 2, compression occurred within approximately $t_c = 10$ fs, and the maximum compression diameter was approximately $D = 30$ nm. The maximum deuterium density exceeded $\rho_m = 1 \times 10^{25}$ cm^{-3}, that is, 120 times the initial ion density. The ion (proton or deuterium) radial flux reached approximately 1.0×10^{34} cm^{-2}s^{-1} ($\rho_m \pi D / t_c$), which is also of intense interest in laboratory nuclear astrophysics research [33–35]. Hence, nanowires can also serve as sources of other nuclear reactions, such as p + ^{11}B → 3α. These ions are concentrated within an extremely small volume of approximately 30 nm × 30 nm and cause intense nuclear reactions, including neutron production. For lasers with $a_0 > 40$, the maximum density of the nanowires increases slightly. For example, with $a_0 = 150$, a maximum density of 1.8×10^{25} cm^{-3} is reached on the front of the wire, owing to an intense axial particle acceleration and the combined effect of the nanowire micro-pinch, which is long before the peak of the laser pulse. When the laser intensity increases, both the magnitude of the return current density and maximum ion density increase, but not indefinitely in our simulation. This would limit the number of nuclear reactions during the Z-pinch (Fig. 4a). This may be caused by instabilities [36], such as sausage or kink instabilities in the Z-pinch effect.

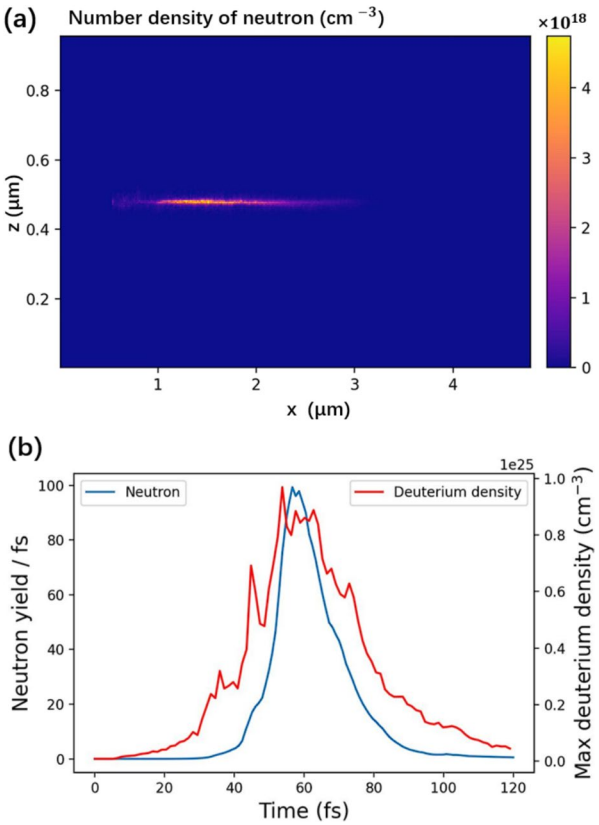

Fig. 3 (Color online) (**a**) Longitudinal cross section of the accumulated neutron number density, which shows the spatial distribution where D–D nuclear reactions occur. (**b**) The number of nuclear reactions produced per femtosecond (the blue curve) and the time evolution of the deuterium maximum density (the red curve). The nanowire has a diameter of 300 nm and a length of 3.6 μm

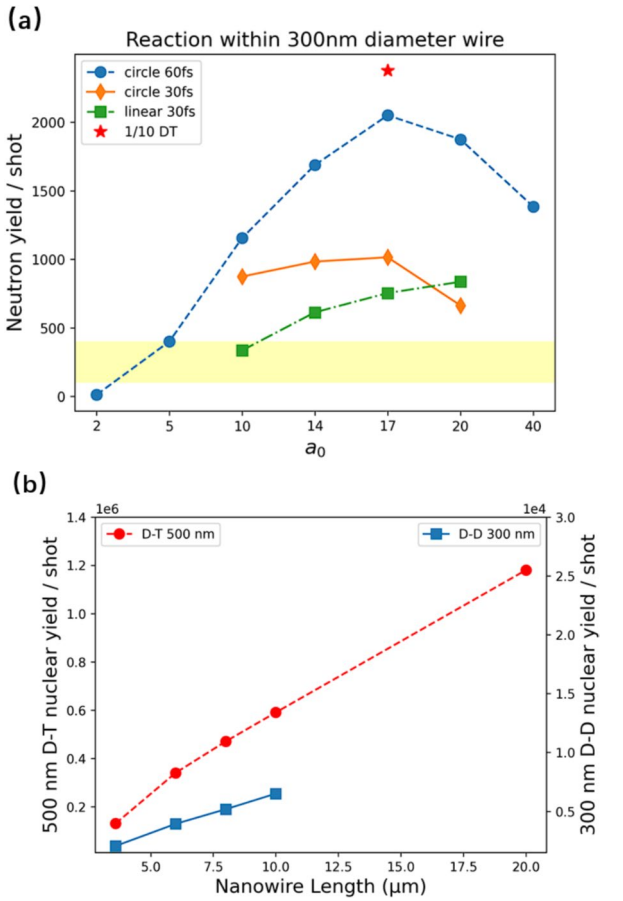

Fig. 4 (Color online) (**a**) Relationship between the number of reactions in a nanowire with a diameter of 300 nm and a length of 3.6 μm and several laser intensities. The blue circle in the diagram represents a 60 fs pulse width circularly polarized laser, whereas the orange and green marks represent 30 fs pulse width circularly or linearly polarized lasers. The yellow range is the approximate range of nuclear reactions that we estimate can be generated by existing Z-pinch devices under the same amount of substance. The red star is one-tenth of the D–T reaction counts. (**b**) Number of fusions with various lengths. The red circle represents D–T fusion, and its yield is on the left. The blue square represents D–D fusion, and its yield is on the right

Figure 3 shows the number and density of nuclear reactions (D + D → n + ^{3}He) generated by the Z-pinch. The propagation of the produced neutrons was not considered. At this point, the energetic ions collide in the densest vicinity. Because of the extremely high particle number density, the nuclear reactions primarily occur around the axis of the nanowire, as shown in Fig. 3a. The neutron density resulting from D–D nuclear reactions is approximately of the order of 10^{18} cm^{-3}. This extremely short compression leads to a burst of reactions within femtoseconds, where the reaction rate is over 100 fs^{-1} on such a small timescale, as shown in Fig. 3b. If suitable nuclear reactions are available, the induced reaction exhibits ultrahigh peak flux and ultrashort pulse duration. From the simulations, we obtained neutrons with a narrow pulse width (30 fs) and small source surface area ($\pi 30\,\text{nm} \times 3000\,\text{nm} = 2.8 \times 10^5\,\text{nm}^2$). The corresponding neutron (particle) flux reached 10^{26} cm^{-2}s^{-1}.

Figure 4a illustrates the relationship between the laser parameters (30 and 60 fs, circularly and linearly polarized, respectively) and the number of nuclear reactions generated by the Z-pinch. In addition, increasing the length efficiently enhances the number of nuclear reactions during the pinch phase. The diameter of the nanowire also affects the reaction rate. Under the same conditions, if normalized for the amount of substance, the efficiency of nuclear reaction generation is the highest in the wire with a diameter of 500 nm, followed by that with a diameter of 300 nm. Both efficiencies were higher than those observed for the 200 nm and 800 nm wires.

When the D–T system was considered, the fusion yield was found to be more than 10 times greater than that of the D–D system. Comparing the yields in the same system, the

equivalent temperature [37] at which the nuclear reactions occurred in this nanowire was approximately 190 keV. The neutron flux could reach 10^{27} $cm^{-2}s^{-1}$ in the D–T reaction system. Nanowires with a diameter of 500 nm and lengths of 6, 8, and 10 µm can generate 3.4×10^5, 4.7×10^5, and 5.9×10^5 neutrons, respectively. Notably, this growth is almost linear with the length. (Because of the pulse width of the laser, it must be sufficiently long.) More than 10^6 neutrons can be generated within a single pulse if the length of the nanowire is increased to 20 µm, as shown in Fig. 4b. Cascade reactions of D–D and D–T also occur within the system.

4 Conclusion

We conducted a study on the interaction between lasers and nanowires, with a particular focus on the Z-pinch effect. Notably, the deuterium density within the nanowire could exceed the initial density by more than 100 times. We analyzed the pinch density and current under different laser and nanowire parameters. The Z-pinch effect provides laser-driven nanowires with a short time scale and high spatial density environment for nuclear reactions to occur. It is thus suitable for use as a neutron source with the advantages of a small spatial scale (30 nm × 30 nm) and short pulse width (30 fs). This compression results in an extremely intense and short neutron pulse. The peak neutron flux reached 10^{27} $cm^{-2}s^{-1}$. High-flux nuclear reaction (neutron) sources can be utilized for research on r processes [38]. The laser can not only pinch deuterium ions but also other particles as sources in nanowires. A typical example is a proton source. With a radial flux of approximately 1.0×10^{34} $cm^{-2}s^{-1}$, the proton source will provide a unique method for the two-proton capture reaction during the rp-process [39]. Future studies could utilize targets with different compositions to conduct further laboratory nuclear astrophysics research [40, 41], which could provide highly intense solutions.

Author Contributions All authors contributed to the study conception and design. Material preparation, data collection and analysis were performed by Pu-tong Wang, Xue-Song Geng, Guo-Qiang Zhang, and Liang-Liang Ji. Funding acquisition, project administration, and resources were performed by Yu-Gang Ma. The first draft of the manuscript was written by Pu-tong Wang, and all authors commented on previous versions of the manuscript. All authors read and approved the final manuscript.

Data Availability The data that support the findings of this study are openly available in Science Data Bank at https://cstr.cn/31253.11.sciencedb.j00186.00673 and https://www.doi.org/10.57760/sciencedb.j00186.00673..

Declarations

Conflict of interest Yu-Gang Ma is the editor-in-chief for Nuclear Science and Techniques and was not involved in the editorial review. All authors declare that there are no conflict of interest.

References

1. I.S. Anderson, C. Andreani, J.M. Carpenter et al., Research opportunities with compact accelerator-driven neutron sources. Phys. Rep. **654**, 1–58 (2016). https://doi.org/10.1016/jphysrep.2016.07.007.
2. J. Wei, H. Chen, Y. Chen et al., China spallation neutron source: Design, r &d, and outlook. Nucl. Instrum. Methods Phys. Res., Sect. A **600**, 10–13 (2009). https://doi.org/10.1016/j.nima.2008.11.017
3. R. Garoby, A. Vergara, H. Danared et al., The european spallation source design. Phys. Scr. **93**, 014001 (2017). https://doi.org/10.1088/1402-4896/aa9bff
4. J.M. Xue, S. Feng, Y.H. Chen et al., Measurement of the neutron-induced total cross sections of ^{nat}Pb from 0.3 eV to 20 MeV on the back-n at CSNS. Nucl. Sci. Tech. **35**, 18 (2024). https://doi.org/10.1007/s41365-024-01370-z
5. G.L. Yang, Z.D. An, W. Jiang et al., Measurement of Br(n, γ) cross sections up to stellar s-process temperatures at the CSNS back-n. Nucl. Sci. Tech. **34**, 180 (2023). https://doi.org/10.1007/s41365-023-01337-6
6. J.J. Cowan, C. Sneden, J.E. Lawler et al., Origin of the heaviest elements: The rapid neutron-capture process. Rev. Mod. Phys. **93**, 015002 (2021). https://doi.org/10.1103/RevModPhys.93.015002
7. F.K. Thielemann, A. Arcones, R. Käppeli et al., What are the astrophysical sites for the r-process and the production of heavy elements? Prog. Part. Nucl. Phys. **66**, 346–353 (2011). https://doi.org/10.1016/j.ppnp.2011.01.032. (**Particle and Nuclear Astrophysics**)
8. E. Pian, P. D'Avanzo, S. Benetti et al., Spectroscopic identification of r-process nucleosynthesis in a double neutron-star merger. Nature **551**, 67–70 (2017). https://doi.org/10.1038/nature24298
9. J. Alvarez, J. Fernández-Tobias, K. Mima, et al., Laser driven neutron sources: Characteristics, applications and prospects. Physics Procedia **60**, 29–38 (2014). https://doi.org/10.1016/j.phpro.2014.11.006
10. A. Taylor, M. Dunne, S. Bennington et al., A route to the brightest possible neutron source? Science **315**, 1092–1095 (2007). https://doi.org/10.1126/science.1127185
11. X. Jiao, J. Shaw, T. Wang et al., A tabletop, ultrashort pulse photoneutron source driven by electrons from laser wakefield acceleration. Matter. Radiat. Extremes **2**, 296–302 (2017). https://doi.org/10.1016/j.mre.2017.10.003
12. K. Ledingham, I. Spencer, T. McCanny et al., Photonuclear physics when a multiterawatt laser pulse interacts with solid targets. Phys. Rev. Lett. **84**, 899–902 (2000). https://doi.org/10.1103/PhysRevLett.84.899
13. M. Roth, D. Jung, K. Falk et al., Bright laser-driven neutron source based on the relativistic transparency of solids. Phys. Rev. Lett. **110**, 044802 (2013). https://doi.org/10.1103/PhysRevLett.110.044802
14. M. Günther, O. Rosmej, P. Tavana et al., Forward-looking insights in laser-generated ultra-intense γ-ray and neutron sources for nuclear application and science. Nat. Commun. **13**, 170 (2022). https://doi.org/10.1038/s41467-021-27694-7
15. A.L. Kritcher, C.V. Young, H.F. Robey et al., Design of inertial fusion implosions reaching the burning plasma regime. Nat. Phys. **18**, 251–258 (2022). https://doi.org/10.1038/s41567-021-01485-9
16. W.H. Bennett, Magnetically self-focussing streams. Phys. Rev. **45**, 890–897 (1934). https://doi.org/10.1103/PhysRev.45.890
17. M.G. Haines, S.V. Lebedev, J.P. Chittenden et al., The past, present, and future of Z pinches. Phys. Plasmas **7**, 1672–1680 (2000). https://doi.org/10.1063/1.874047

18. M.G. Haines, A review of the dense z-pinch. Plasma Phys. Controlled Fusion **53**, 093001 (2011). https://doi.org/10.1088/0741-3335/53/9/093001
19. V. Kantsyrev, A. Safronova, A. Esaulov et al., A review of new wire arrays with open and closed magnetic configurations at the 1.6 MA Zebra generator for radiative properties and opacity effects. High Energy Density Phys. **5**, 115–123 (2009). https://doi.org/10.1016/j.hedp.2009.04.001
20. D.D. Ryutov, M.S. Derzon, M.K. Matzen, The physics of fast z pinches. Rev. Mod. Phys. **72**, 167–223 (2000). https://doi.org/10.1103/RevModPhys.72.167
21. K.K. Ostrikov, F. Beg, A. Ng, Colloquium: Nanoplasmas generated by intense radiation. Rev. Mod. Phys. **88**, 011001 (2016). https://doi.org/10.1103/RevModPhys.88.011001. (**Publisher: American Physical Society**)
22. V. Kaymak, A. Pukhov, V.N. Shlyaptsev et al., Nanoscale ultradense z-pinch formation from laser-irradiated nanowire arrays. Phys. Rev. Lett. **117**, 035004 (2016). https://doi.org/10.1103/PhysRevLett.117.035004
23. J.J. Rocca, M.G. Capeluto, R.C. Hollinger et al., Ultra-intense femtosecond laser interactions with aligned nanostructures. Optica **11**, 437 (2024). https://doi.org/10.1364/OPTICA.510542
24. C. Bargsten, R. Hollinger, M.G. Capeluto et al., Energy penetration into arrays of aligned nanowires irradiated with relativistic intensities: Scaling to terabar pressures. Sci. Adv. **3**, e1601558 (2017). https://doi.org/10.1126/sciadv.1601558
25. Y. Shou, D. Kong, P. Wang et al., High-efficiency water-window x-ray generation from nanowire array targets irradiated with femtosecond laser pulses. Opt. Express **29**, 5427–5436 (2021). https://doi.org/10.1364/OE.417512.
26. A. Curtis, C. Calvi, J. Tinsley et al., Micro-scale fusion in dense relativistic nanowire array plasmas. Nat. Commun. **9**, 1077 (2018). https://doi.org/10.1038/s41467-018-03445-z
27. J. Derouillat, A. Beck, F. Pérez et al., Smilei: A collaborative, open-source, multi-purpose particle-in-cell code for plasma simulation. Comput. Phys. Commun. **222**, 351–373 (2018). https://doi.org/10.1016/j.cpc.2017.09.024
28. D.P. Higginson, A. Link, A. Schmidt, A pairwise nuclear fusion algorithm for weighted particle-in-cell plasma simulations. J. Comput. Phys. **388**, 439–453 (2019). https://doi.org/10.1016/j.jcp.2019.03.020
29. D.P. Higginson, I. Holod, A. Link, A corrected method for coulomb scattering in arbitrarily weighted particle-in-cell plasma simulations. J. Comput. Phys. **413**, 109450 (2020). https://doi.org/10.1016/j.jcp.2020.109450
30. Z. Zhu, J. Xu, G.Q. Zhang, Simulating fusion reactions from coulomb explosions within a transport approach. Phys. Rev. C **106**, 034604 (2022). https://doi.org/10.1103/PhysRevC.106.034604
31. National Nuclear Data Center. https://www.nndc.bnl.gov/
32. D. Kong, G. Zhang, Y. Shou et al., High-energy-density plasma in femtosecond-laser-irradiated nanowire-array targets for nuclear reactions. Matter Radiat. Extremes **7**, 064403 (2022). https://doi.org/10.1063/5.0120845
33. Z.L. Shen, J.J. He, Study of primordial deuterium abundance in big bang nucleosynthesis. Nucl. Sci. Tech. **35**, 63 (2024). https://doi.org/10.1007/s41365-024-01423-3
34. Y.J. Chen. L.Y. Zhang, Examining the fluorine overabundance problem by conducting jinping deep underground experiment. Nucl. Tech. (in Chinese) **46**, 110501 (2023). https://doi.org/10.11889/j.0253-3219.2023.hjs.46.110501
35. J.Y.H. Li, Y.J. Li, Z.H. Li et al., Nuclear astrophysics research based on HI-13 tandem accelerator. Nucl. Tech. (in Chinese) **46**, 080002 (2024). https://doi.org/10.11889/j.0253-3219.2023.hjs.46.080002
36. M.G. Haines, M. Coppins, Universal diagram for regimes of z-pinch stability. Phys. Rev. Lett. **66**, 1462–1465 (1991). https://doi.org/10.1103/PhysRevLett.66.1462
37. W. Bang, M. Barbui, A. Bonasera et al., Temperature measurements of fusion plasmas produced by petawatt-laser-irradiated $\mathbf{D}_2$−^{3}He or CD_4−^{3}He clustering gases. Phys. Rev. Lett. **111**, 055002 (2013). https://doi.org/10.1103/PhysRevLett.111.055002
38. J.J. Cowan, C. Sneden, J.E. Lawler et al., Origin of the heaviest elements: The rapid neutron-capture process. Rev. Mod. Phys. **93**, 015002 (2021). https://doi.org/10.1103/RevModPhys.93.015002
39. H. Schatz, A. Aprahamian, J. Görres et al., rp-process nucleosynthesis at extreme temperature and density conditions. Phys. Rep. **294**, 167–263 (1998). https://doi.org/10.1016/S0370-1573(97)00048-3
40. W.P. Liu, B. Guo, Z. An et al., Recent progress in nuclear astrophysics research and its astrophysical implications at the china institute of atomic energy. Nucl. Sci. Tech. **35**, 217 (2024). https://doi.org/10.1007/s41365-024-01590-3
41. W.K. Nan, Y.B. Wang, Y.D. Sheng et al., Novel thick-target inverse kinematics method for the astrophysical 12c+12c fusion reaction. Nucl. Sci. Tech. **35**, 208 (2024). https://doi.org/10.1007/s41365-024-01573-4